IOPscience iopscience.iop.org

Home Search Collections Journals About Contact us My IOPscience

A pseudo-Jahn - Teller vibronic model of d^3 ions in cubic crystals; the luminescence band shape and lifetimes of $CdIn_2S_4:Cr^{3+}$

This article has been downloaded from IOPscience. Please scroll down to see the full text article.

1997 J. Phys.: Condens. Matter 9 5295

(http://iopscience.iop.org/0953-8984/9/25/001)

View the table of contents for this issue, or go to the journal homepage for more

Download details:
IP Address: 171.66.16.207
The article was downloaded on 14/05/2010 at 08:59

Please note that terms and conditions apply.

J. Phys.: Condens. Matter **9** (1997) 5295–5312. Printed in the UK PII: S0953-8984(97)76617-7

A pseudo-Jahn–Teller vibronic model of d^3 ions in cubic crystals; the luminescence band shape and lifetimes of $CdIn_2S_4:Cr^{3+}$

B S Tsukerblat†, A V Palii†, S M Ostrovsky†, L L Kulyuk‡ and S M Popov‡

† Institute of Chemistry, Academy of Sciences of Moldova, Academy Street 3, MD-2028, Chisinau, Moldova

‡ Institute of Applied Physics, Academy of Sciences of Moldova, Academy Street 5, MD-2028, Chisinau, Moldova

Received 23 July 1996, in final form 23 January 1997

Abstract. A new model for the vibronic problem of the luminescence of $3d^3$ impurity ions in the cubic environment is proposed. The approach developed is based on the numerical quantum-mechanical solution of the dynamic pseudo-Jahn–Teller vibronic problem for the excited states. The spin–orbit splitting of the $^4T_2$ term, and its mixing with ^2E, as well as the vibronic interaction with the full-symmetric (A_{1g}) local mode, are taken into account, resulting in the $(\Gamma_8 + \Gamma_8' + \Gamma_8'') \otimes a_1$ vibronic problem, and the $\Gamma_6 \otimes a_1$ and $\Gamma_7 \otimes a_1$ adiabatic problems. The effective dipole moment operator is built with due regard for a weak odd-parity trigonal crystal-field component. The vibronic wave-functions are used for the calculation of the band shape of the luminescence in the R line and U band, as well as for the evaluation of the temperature dependence of the lifetime decay emission of Cr^{3+} ions in $CdIn_2S_4$:Cr single crystals. The proposed model provides a very good explanation of the experimental data.

1. Introduction

The Cr^{3+} ion plays an important role in laser-type solid-state materials. It can be used directly as an active centre in tunable laser materials [1–3] in the near-infrared spectral region, and as a sensitizer in rare-earth-doped host materials. The electronic energy levels of this ion are determined by the interaction of 3d electrons with the electrostatic field of the host lattice [4].

Absorption and emission spectra of the octahedrally coordinated Cr^{3+} ion in the visible region can be illustrated by the well known model of the adiabatic potentials [5, 6], as shown in figure 1(a), where Q is the full-symmetric coordinate (the breathing mode) of the local surroundings of the Cr^{3+} in crystal. The vibrational relaxation accompanying the optical $^4A_2(t_2^3) \rightarrow {}^4T_2(t_2^2e)$ excitation results in the strong full-symmetric lattice deformation due to the change of the electronic configuration, $t_2^3 \rightarrow t_2^2e$, giving rise to a broad U band of absorption and emission. The general pattern of the adiabatic potentials of the excited ^2E_g, $^2T_{2g}$ manifold closely depends on two key parameters of the system: the cubic crystal-field parameter Dq and the vibronic interaction. Systematic changes of the crystal-field strength have been observed for a series of garnets, $A_3B_2C_3O_{12}$ [6], by means of variation of the crystal composition.

0953-8984/97/255295+18$19.50 © 1997 IOP Publishing Ltd

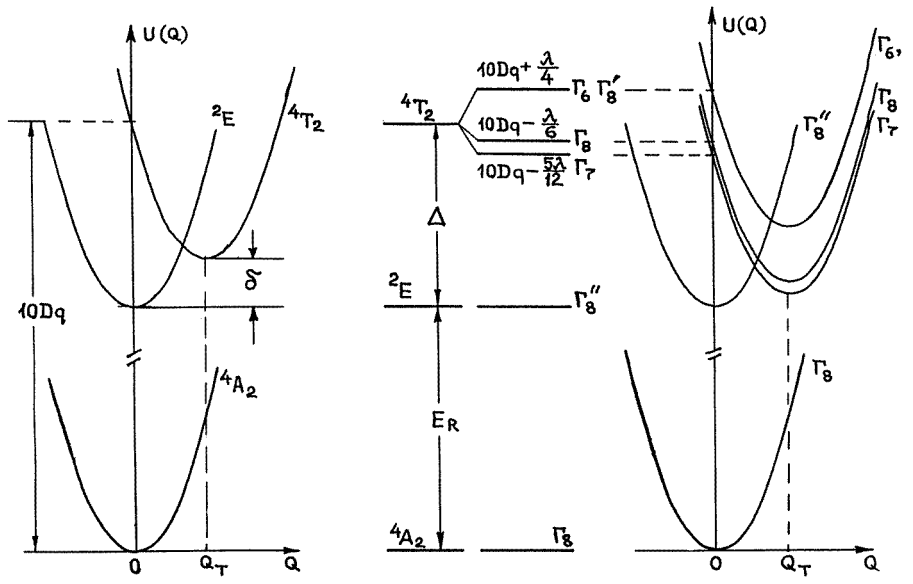

Figure 1. Adiabatic potentials of Cr^{3+} ions in cubic surroundings; Q is the full-symmetric local coordinate. (a) The spin–orbit interaction is neglected. (b) The spin–orbit splitting of $^4T_2(t_2^2e)$. (c) The adiabatic potentials of $^4T_2$ split by spin–orbit interaction (a first-order effect).

Much less is known about the vibronic parameter determining (along with Dq) the relative position of the minima of the ^2E and $^4T_2$ terms (the potentials $U^{(^2E)}(Q)$ and $U^{(^4T_2)}(Q)$ in figure 1(a)). In the case of a strong crystal field and a relatively strong vibronic interaction, the ^2E well is considerably deeper than that for $^4T_2$, and these wells are separated by a high barrier, suppressing the tunnelling processes. In many crystals with strong cubic crystal fields, the typical values of the decay times for the luminescence in the phonon-assisted broad U band and zero-phonon R line are observed to be approximately 10^{-5} s and 10^{-3} s respectively [5]. The non-vanishing intensity of the emission in the R line (the spin-forbidden $^2E \rightarrow {}^4A_2$ transition) arises from spin–orbit $^4T_2$–^2E mixing, so the ratio of the decay lifetimes $\tau(R)/\tau(U)$ can be roughly estimated as $(\lambda/\Delta)^2$ where λ is the spin–orbit coupling and Δ is the gap $\varepsilon(^4T_2) - \varepsilon(^2E)$ in the static lattice (figure 1). When the barrier separating $U^{(^2E)}(Q)$ and $U^{(^4T_2)}(Q)$ wells is high, the spin–orbit mixing of the ground vibronic levels in these wells is negligible (due to the small overlap of the vibrational wave-functions) even if the gap δ between the minima $U^{(^2E)}$ and $U^{(^4T_2)}$ is small (figure 1(a)). In the case of a high barrier, the adiabatic approximation for several thermally populated ground vibronic levels of ^2E and $^4T_2$ (originating in the emission) works well.

In the case of a moderate crystal field and intermediate vibronic coupling, the well of the ^2E term remains the ground state, giving rise to an observable R emission in the tail of the U band of the luminescence, the intensities of the R and U emission bands being comparable. But, in this case, the gap δ is relatively small, as is the barrier between the wells of ^2E and $^4T_2$, giving rise to an anomalous ratio for the lifetimes $\tau(R)/\tau(U)$, and anomalous intensities in the luminescence spectra. Under these conditions, the non-adiabatic problem for excited states arises, and the ground vibronic levels of $U^{(^2E)}$ and $U^{(^4T_2)}$ are mixed. The important idea of tunnelling has been proposed in [7] and developed in [8, 9] in order

to explain these peculiarities. The ground vibronic levels of $U^{(^2\mathrm{E})}(Q)$ and $U^{(^4\mathrm{T}_2)}(Q)$ are assumed to be vibronically mixed, which does in fact prove to be possible due to spin–orbit interaction. The idea of vibronic mixing (tunnelling) is fruitful, but the semiempirical model used so far [7–9] should be generalized. In fact, in the model of [7–9] only two ground vibrational levels are mixed, and the spin–orbit interaction as well the off-diagonal part of the Hamiltonian have been modelled by the only off-diagonal matrix element in the 2×2 matrix of mixing (tunnelling), the spin–orbit splitting of $^4\mathrm{T}_2$ being neglected.

The real physical situation for the excited states for $3d^3$ impurities is much more complicated. In fact, all of the physical parameters involved in determining the lifetimes and band shape of the luminescence—namely, the barrier between $U^{(^2\mathrm{E})}(Q)$ and $U^{(^4\mathrm{T}_2)}(Q)$ ($\approx$200 cm^{-1} for $Gd_3Sc_2Ga_3O_{12}$:Cr^{3+} [8]), the spin–orbit interaction parameter ($\lambda \approx$ 100 cm^{-1} for Cr^{3+} [7]), and a typical energy for active vibrational quanta ($\bar{h}\omega \sim$ 300–400 cm^{-1} [3]) are comparable. This is just the case when the conditions of validity for the adiabatic approximation are broken, and the vibrational kinetic energy should be taken into consideration as well as the spin–orbit interaction. In this way we arrive at a non-adiabatic spin-vibronic problem, in which all relevant interactions should be taken into account simultaneously.

Here we propose a general model for the vibronic problem of luminescence from the excited states of Cr^{3+} in the cubic environment. At the same time we assume that a weak odd crystal field makes the electric dipole transitions partially allowed, but does not significantly affect the pattern of cubic field levels. We develop the approach based on the numerical quantum-mechanical solution of the dynamic pseudo-Jahn–Teller vibronic problem, with allowance made for the spin–orbit splitting of the $^4\mathrm{T}_2$ term and its mixing with the $^2\mathrm{E}$ term. The electron–vibrational (vibronic) wave-functions and energy levels of the system thus obtained are used for the calculation of the form functions of the luminescence bands corresponding to the transitions from hybrid vibronic states belonging to the $^4\mathrm{T}_2 + {}^2\mathrm{E}$ manifold into the ground state $^4\mathrm{A}_2$, as well as for the evaluation of the temperature dependence of the decay lifetime of Cr^{3+} ions in cubic crystals. The proposed model is applied to chromium-doped $CdIn_2S_4$ single crystals, neglecting the trigonal component of the crystal field.

2. Theory

2.1. Spin–orbit interaction in the excited states of $3d^3$ ions in a cubic field

The Hamiltonian of a doped crystal can be presented as

$$H = H_e(\boldsymbol{r}) + H_L(q) + H_{ev}(\boldsymbol{r}, q) \tag{1}$$

where the electronic part $H_e = H_c + H_{SO}$ contains the crystal-field Hamiltonian H_c and the spin–orbit interaction H_{SO} ($\boldsymbol{r}$ represents the set of electronic coordinates, and q the vibrational ones). H_L is the Hamiltonian of free lattice vibrations, and H_{ev} is the electron–vibrational (vibronic) interaction for the impurity ion.

In the cubic-crystal-field approximation, three terms, $^4\mathrm{A}_{2g}(t_2^3)$, $^2\mathrm{E}_g(t_2^3)$, and $^4\mathrm{T}_{2g}(t_2^2e)$, participate in the photoluminescence processes (figure 1(a)). Spin–orbit interaction splits the $^4\mathrm{T}_2$ term according to the scheme $^4\mathrm{T}_2 \doteq \Gamma_8 + \Gamma_8' + \Gamma_6 + \Gamma_7$ [9], and also mixes $^2\mathrm{E}(\Gamma_8'')$ with the Γ_8 and Γ_8' components of $^4\mathrm{T}_2$, giving rise to a non-vanishing intensity for the spin-forbidden R line (here and further on, the symbol 'g' for the parity is omitted, and Bethe's notation is used for the double-valued irreducible representations of O_h).

The spin–orbit interaction operator can be presented as [3]

$$H_{SO} = \sum_i \lambda(\boldsymbol{r}_i)\boldsymbol{s}_i \cdot \boldsymbol{l}_i \tag{2}$$

where the summation involves the electrons of the unfilled d^n shell. The crystal-field wave-functions $|\alpha S\Gamma M\gamma\rangle$ of the d^3 shell, expressed in terms of Slater's determinants, are given in [4] (S, M are the quantum numbers of the full spin and its projection, Γ, γ label the irreducible representation and basis functions respectively, and $\alpha = t_2^n e^{3-n}$). Using the explicit expressions for the wave-functions $|t_2^2 e\,{}^4T_2\rangle$ and $|t_2^3\,{}^2E\rangle$, as well as the approach based on the theory of irreducible tensors and described in [4] in detail (see also [10]), we find the matrix of H_{SO} in the basis of $^4T_{2g}(t_2^2e)$, and the matrix of the spin–orbit mixing $^4T_{2g}(t_2^2e)$–$^2E_g(t_2^3)$ (see equations (7.50), (7.65) in reference [4]). The matrix elements of H_{SO} contain two parameters ζ_1 and ζ_2 (ζ and ζ' in the notation of [4]); these parameters are expressed in terms of the matrix elements of $\lambda(\boldsymbol{r})$ in the basis of t_2 functions (parameter ζ_1) and t_2–e mixing (parameter ζ_2) (see equation (7.13) and p 175 in [4]).

The matrices of the spin–orbit interactions $\langle\alpha S\Gamma M\gamma|H_{SO}|\alpha' S'\Gamma' M'\gamma'\rangle$ can be reduced in the symmetry-adapted basis corresponding to the double-valued representations of the O_h group. The wave-functions of the fine-structure levels corresponding to the double-valued irreducible representation Γ_i are obtained from the initial $S\Gamma$ states ($S\Gamma = {}^2E$, $^4T_2$) by means of the unitary transformation [10]

$$|\alpha S\Gamma;\Gamma_i\gamma_i\rangle = \sum_{\gamma_S\gamma} |\alpha S\Gamma\gamma_S\gamma\rangle\langle\Gamma_S\gamma_S\Gamma\gamma|\Gamma_i\gamma_i\rangle \tag{3}$$

where Γ_i are the double-valued representations, γ_i enumerate the basis functions of Γ_i, Γ_S are the double-valued irreducible representations with the bases corresponding to the spin components for $S = \frac{3}{2}$ ($^4T_2$) and $S = \frac{1}{2}$ (^2E_g), the γ_S enumerate the basis functions of Γ_S (the values of the full spin projections), $\Gamma_{1/2} = \Gamma_6$, $\Gamma_{3/2} = \Gamma_8$ ($\gamma_{1/2} = \pm\frac{1}{2}$, $\gamma_{3/2} = \pm\frac{1}{2}, \pm\frac{3}{2}$), and $\langle\Gamma_S\gamma_S\Gamma\gamma|\Gamma_i\gamma_i\rangle$ are the Clebsch–Gordan coefficients of the double group O_h (which are given in [11]). Using equation (3), one can obtain the wave-functions of the fine-structure levels of the $^4T_{2g}$ (t_2^2e) term in the following form:

$$\begin{aligned}
\left|\Gamma_8, \pm\frac{3}{2}\right\rangle &= \sqrt{\frac{4}{15}}\varphi_\pm\left(\pm\frac{1}{2}\right) + \frac{1}{\sqrt{5}}\varphi_\mp\left(\mp\frac{3}{2}\right) \mp \frac{\mathrm{i}}{\sqrt{15}}\left|\zeta, \mp\frac{1}{2}\right\rangle \\
\left|\Gamma_8, \pm\frac{1}{2}\right\rangle &= -\frac{1}{\sqrt{5}}\varphi_\pm\left(\mp\frac{1}{2}\right) \pm \mathrm{i}\sqrt{\frac{3}{5}}\left|\zeta, \mp\frac{3}{2}\right\rangle \\
\left|\Gamma_8', \pm\frac{3}{2}\right\rangle &= -\sqrt{\frac{3}{20}}\varphi_\pm\left(\pm\frac{1}{2}\right) + \frac{1}{\sqrt{20}}\varphi_\mp\left(\mp\frac{3}{2}\right) \mp \mathrm{i}\sqrt{\frac{3}{5}}\left|\zeta, \mp\frac{1}{2}\right\rangle \\
\left|\Gamma_8', \pm\frac{1}{2}\right\rangle &= \sqrt{\frac{5}{12}}\varphi_\mp\left(\pm\frac{3}{2}\right) - \frac{1}{\sqrt{20}}\varphi_\pm\left(\mp\frac{1}{2}\right) \mp \frac{\mathrm{i}}{\sqrt{15}}\left|\zeta, \mp\frac{3}{2}\right\rangle \\
\left|\Gamma_7, \pm\frac{1}{2}\right\rangle &= \pm\frac{1}{2}\varphi_\pm\left(\pm\frac{3}{2}\right) \mp \frac{1}{\sqrt{12}}\varphi_\mp\left(\mp\frac{1}{2}\right) - \frac{\mathrm{i}}{\sqrt{3}}\left|\zeta, \pm\frac{1}{2}\right\rangle \\
\left|\Gamma_6, \pm\frac{1}{2}\right\rangle &= \mp\frac{1}{\sqrt{12}}\varphi_\mp\left(\pm\frac{3}{2}\right) \mp \frac{1}{2}\varphi_\pm\left(\mp\frac{1}{2}\right) - \frac{\mathrm{i}}{\sqrt{3}}\left|\zeta, \mp\frac{3}{2}\right\rangle
\end{aligned} \tag{4}$$

where $\varphi_\pm(\gamma_S)$ are the cyclic components of $^4T_2$ related to the C_4 axis (figure 2):

$$\mathrm{i}|\xi, \gamma_S\rangle \pm |\eta, \gamma_S\rangle \equiv \varphi_\pm(\gamma_S).$$

The following shorthand notation is also used in equations (4):

$$\left|{}^4T_2(t_2^2e),\,\Gamma_8,\,\gamma_{3/2}=-\frac{3}{2}\right\rangle \equiv \left|\Gamma_8,\,-\frac{3}{2}\right\rangle \qquad \text{etc.}$$

The wave-functions of Γ'' arising from ${}^2E(t_2^3)$ are the following:

$$\left|\Gamma_8'',\pm\frac{3}{2}\right\rangle = \mp\left|v,\mp\frac{1}{2}\right\rangle \qquad \left|\Gamma_8'',\pm\frac{1}{2}\right\rangle = \mp\left|u,\pm\frac{1}{2}\right\rangle \tag{5}$$

where

$$\left|{}^2E(t_2^3),\,\Gamma_8'',\,\gamma_{3/2}=-\frac{3}{2}\right\rangle \equiv \left|\Gamma_8'',\,-\frac{3}{2}\right\rangle \qquad \text{etc.}$$

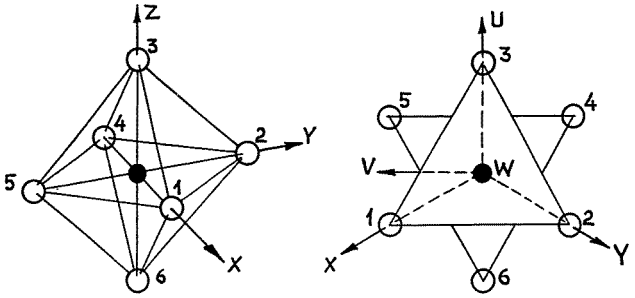

(a) (b)

Figure 2. The octahedral surroundings of Cr^{3+} ions in a crystal: (a) the tetragonal coordinate system; and (b) the trigonal coordinate system.

The first order spin–orbit splitting of the ${}^4T_2(t_2^2e)$ term is shown in figure 1(b). The second-order effect due to ${}^2E$–${}^4T_2$ mixing removes the accidental Γ_8', Γ_6 degeneracy, and leads to additional stabilization of Γ_8''.

2.2. Vibronic interaction

Under the optical excitation of the system in the region of the U band (${}^4A_2(t_2^3) \rightarrow {}^4T_2(t_2^2e)$), a one-electron transition, $t_2^3 \rightarrow t_2^2e$, occurs, and is accompanied by strong deformation of the Cr^{3+}-ion crystal surroundings. The dominant effect is the shift of the equilibrium position of the full-symmetric vibrational coordinate (the A_{1g} mode) [12]. Numerical calculations of the vibronic coupling parameters [12, 13] for the Cr^{3+} ion in ruby showed that the contribution of the full-symmetric A_1 modes in the second moment of the U band is approximately 85% of the total value of $\langle\Omega^2\rangle$; meanwhile the contribution of the Jahn–Teller vibrations (E_g and T_{2g} modes) is estimated as 15% of $\langle\Omega^2\rangle$. This is why here we confine ourselves to a simplified vibronic model, taking only the local A_1 mode into account. Therefore we neglect the interaction with the Jahn–Teller E and T_2 modes (the Jahn–Teller problem of the U-band absorption is considered in [14]), and the operator of the linear electron–vibrational interaction is presented in the following form:

$$\hat{H}_{ev} = V(\boldsymbol{r})q. \tag{6}$$

Here $q \equiv q_{A_1}$ is the full-symmetric coordinate of the octahedral local surroundings of Cr^{3+} in the crystal lattice:

$$q = \frac{1}{l_0\sqrt{6}}(X_1 - X_4 + Y_2 - Y_5 + Z_3 - Z_6) \tag{7}$$

where X_i, Y_i, and Z_i are the Cartesian displacements of the local surroundings of the impurity ion (the enumeration of the ligands, and the coordinate system are shown in figure 2), and $l_0 = (\hbar/M\omega)^{1/2}$, so q is a dimensionless coordinate (ω is the frequency of vibration, and M is its effective mass).

The potential function $V(\boldsymbol{r})$ (having the dimension of energy) can be expressed as a derivative at $q = 0$:

$$\sum_{i,\alpha} \frac{\partial W(|\boldsymbol{r}_i - \boldsymbol{R}_\alpha|)}{\partial q}\bigg|_{q=0}$$

where $W(|\boldsymbol{r}_i - \boldsymbol{R}_\alpha|)$ is the potential energy of the interaction of the ith electron of the chromium ion with the αth atom of the host crystal. In the point-charge crystal-field model, $W_c(|\boldsymbol{r}_i - \boldsymbol{R}_\alpha|)$ is the crystal-field potential acting on the $3d^3$ shell of the impurity ion. Using the explicit form of the q-vibration (equation (6)), one can see that

$$V(\boldsymbol{r}) = l_0 \frac{\partial}{\partial R_0} \sum_i W_c(|\boldsymbol{r}_i - \boldsymbol{R}_0|) \tag{8}$$

where the cubic crystal-field potential $W_c(\boldsymbol{r}_i - \boldsymbol{R}_0)$ depends only on the distance R_0 between the position of the impurity ion and the neighbouring ions. It should be noted that the distance R_0 determined in this way relates to the host lattice unperturbed by the electrons of the 3d shell of the impurity ion.

The matrix elements of $V(\boldsymbol{r})$ can easily be expressed in terms of one-electron contributions. These matrix elements depend on the occupation numbers for t_2 and e shells in the $S\Gamma$-terms:

$$\langle t_2^m e^n S\Gamma M\gamma | V(\boldsymbol{r}) | t_2^m e^n S\Gamma M\gamma \rangle = m v_t + n v_e \tag{9}$$

where v_t and v_e are the one-electron matrix elements of $V(\boldsymbol{r})$ in the T_2 and E bases of the d functions:

$$\begin{aligned} v_t &= \langle \xi | V(\boldsymbol{r}) | \xi \rangle = \langle \eta | V(\boldsymbol{r}) | \eta \rangle = \langle \zeta | V(\boldsymbol{r}) | \zeta \rangle \\ v_e &= \langle u | V(\boldsymbol{r}) | u \rangle = \langle v | V(\boldsymbol{r}) | v \rangle. \end{aligned} \tag{10}$$

The values v_t and v_e play the role of the partial (one-orbital) contributions to the vibronic coupling parameter related to the electrons occupying the t_2 and e orbitals respectively.

In the case of the $3d^3$ shell under consideration, we obtain

$$\begin{aligned} &\langle {}^4T_2(t_2^2 e)\Gamma M\gamma | V(\boldsymbol{r}) | {}^4T_2(t_2^2 e)\Gamma M\gamma \rangle = 2v_t + v_e \\ &\langle {}^4A_2(t_2^3)\Gamma M\gamma | V(\boldsymbol{r}) | {}^4A_2(t_2^3)\Gamma M\gamma \rangle = 3v_t. \end{aligned} \tag{11}$$

In the crystal-field approximation, using equation (9) one can find

$$v_t = -4l_0 \frac{\partial}{\partial R_0} Dq_0 \qquad v_e = 6l_0 \frac{\partial}{\partial R_0} Dq_0 \tag{12}$$

where Dq_0 is the crystal-field parameter defined as usual [9]:

$$\langle t_2 | H_c | t_2 \rangle = -4Dq_0 \qquad \langle e | H_c | e \rangle = 6Dq_0. \tag{13}$$

It should be noted that the parameter Dq_0 as so far defined (labelled with the subscript 0) relates to the positions R_0 of the surrounding ions in the host lattice, i.e. in the lattice without electrons of the unfilled shell of the impurity ion.

In the case of an orbitally non-degenerate ground state ($^4A_2$ in the case under consideration), well separated from the excited ones, the original Hamiltonian (1) can be transformed in order to take into account the shifts of the ions caused by the impurity

electronic shell in its ground state. This shift can be found from the adiabatic potential expression for the $^4A_2(t_2^3)$ term:

$$U_A(q) = \frac{\hbar\omega}{2}q^2 + 3v_t q$$

where ω is the vibrational frequency. The equilibrium position q_A can be expressed as

$$q_A = -\frac{3v_t}{\hbar\omega}. \tag{14}$$

The Hamiltonian (1) can be presented as follows:

$$H = H_0 + H'_{ev} \tag{15}$$

where the new zeroth-order Hamiltonian H_0 is the following:

$$H_0 = H_e(\boldsymbol{r}) + V(\boldsymbol{r})q_A + \frac{\hbar\omega}{2}q_A^2 + \frac{\hbar\omega}{2}\left[(q-q_A)^2 - \frac{\partial^2}{\partial(q-q_A)^2}\right]. \tag{16}$$

The redetermined vibronic interaction is

$$H'_{ev} = (V(\boldsymbol{r}) + \hbar\omega q_A)(q - q_A) \equiv v(\boldsymbol{r})Q \tag{17}$$

where $Q = q - q_A$ is the shifted full-symmetric dimensionless coordinate of the local A_1 mode, and $v(\boldsymbol{r}) = V(\boldsymbol{r}) + \hbar\omega q_A$ is the vibronic potential function adapted to the new equilibrium positions q_A of the ions in the ground electronic state $^4A_2$. The explicit form of $v(\boldsymbol{r})$ shows that the mean value of $v(\boldsymbol{r})$ in the ground state vanishes:

$$\langle {}^4A_2(t_2^3)|v(\boldsymbol{r})|{}^4A_2(t_2^3)\rangle = 0 \tag{18}$$

ensuring that the equilibrium position of the new coordinate Q in the ground state $^4A_2$ is zero ($Q_A = 0$), and so H'_{ev} is the vibronic interaction adapted to the positions of the ions shifted by the $3d^3$ shell. Only this vibronic interaction has real physical meaning for the impurity centre in a cubic crystal.

The ground-state eigenfunction of H_0 is the adiabatic function belonging to the ground electronic state $^4A_2$:

$$|{}^4A_2(t_2^3)\rangle\Phi_n(Q). \tag{19}$$

Here, $\Phi_n(Q)$ is the harmonic oscillator wave-function with quantum number n. The corresponding adiabatic eigenvalues are the following:

$$\varepsilon_n({}^4A_2) = -12Dq_0 - \frac{\hbar\omega}{2}q_A^2 + \hbar\omega\left(n+\frac{1}{2}\right) \equiv -12Dq_0 - \frac{9v_t^2}{2\hbar\omega} + \hbar\omega\left(n+\frac{1}{2}\right). \tag{20}$$

The first term in (20) is the crystal-field energy, and the second one is the potential energy gain due to the interaction between the t_2^3 electronic shell in the $^4A_2$ state and the crystal environment shifted to the position q_A. Using equation (11), one can find the matrix elements of H'_{ev} in the $^4T_2(t_2^2e)$ basis:

$$\langle {}^4T_2(t_2^2e)\Gamma M\gamma|H'_{ev}|{}^4T_2(t_2^2e)\Gamma M\gamma\rangle = vQ \tag{21}$$

where $v = v_e - v_t$ is the vibronic parameter determining the shift of the coordinate Q accompanying the optical excitation $^4A_2(t_2^3) \rightarrow {}^4T_{2g}(t_2^2e)$ (the $t_2 \rightarrow e$ one-electron transition). The new position Q_T of the surrounding ions will be (figure 1(a))

$$Q_T = -\frac{v_e - v_t}{\hbar\omega}. \tag{22}$$

Equation (22) shows that $v = v_e - v_t$ is the only physical parameter of the vibronic interaction that is closely related to the difference between the spatial electronic distributions

in the e and t_2 d states. It is important to note that this parameter can be expressed as a derivative of the crystal-field parameter $10Dq$ (equations (13)):

$$v = \frac{\partial}{\partial R_0} 10Dq_0 = -\frac{5}{R_0} 10Dq_0.$$

This expression can be used in order to establish a correlation between the crystal-field parameter and the vibronic constant for the series of crystals.

Table 1. The matrix of the vibronic and spin–orbit interaction for the $^4T_2$, ^2E manifold, in the basis of the double-valued irreducible representations (symbols enumerating the basis functions are omitted). Within the matrix, X stands for $vQ + 10Dq$.

	$^4T_2$, Γ_8	$^4T_2$, Γ_8'	^2E, Γ_8''	$^4T_2$, Γ_6	$^4T_2$, Γ_7
$^4T_2$, Γ_8	$-\frac{\zeta_1}{6} + X$	0	$-\sqrt{\frac{2}{15}}\,\zeta_2$	0	0
$^4T_2$, Γ_8'	0	$\frac{\zeta_1}{4} + X$	$-\sqrt{\frac{6}{5}}\,\zeta_2$	0	0
^2E, Γ_8''	$-\sqrt{\frac{2}{15}}\,\zeta_2$	$-\sqrt{\frac{6}{5}}\,\zeta_2$	E_R	0	0
$^4T_2$, Γ_6	0	0	0	$\frac{\zeta_1}{4} + X$	0
$^4T_2$, Γ_7	0	0	0	0	$-\frac{5\zeta_1}{12} + X$

The electron–vibrational energy levels of $^4T_2$ can be found in the adiabatic approach, neglecting the spin–orbit splitting in $^4T_2$, and the $^4T_2$–^2E mixing:

$$\varepsilon_n'(^4T_2) = -2Dq_0 - \frac{(v_t - v_e)^2}{2\hbar\omega} + \hbar\omega\left(n' + \frac{1}{2}\right). \tag{23}$$

In the adiabatic approach, the gap

$$\hbar\omega_m(\mathrm{U}) = 10Dq_0 + \frac{9v_t^2}{2\hbar\omega} \tag{24}$$

is the energy of the maximum of the U band, which should be attributed to the magnitude of $10Dq$. As distinct from $10Dq_0$ (equations (13)), the value $10Dq$ is determined afresh as a result of the electrons of the impurity shifting the ligands to the position q_A. In fact, this value is just the observable $10Dq$ corresponding to the first moment of light absorption in the U band (i.e. roughly to the maximum of the U band). Taking into account the spin–orbit interaction in the excited $^2E(t_2^3)$, $^4T_2(t_2^2e)$ manifold, we arrive at a non-adiabatic dynamic spin-vibronic problem involving spin–orbit and vibronic mixing in the excited states. The matrix Hamiltonian of the excited $^4T_2$, ^2E manifold can be expressed as

$$\mathbf{H} = \frac{\hbar\omega}{2}\left(Q^2 - \frac{\partial^2}{\partial Q^2}\right)\mathbf{1} + \mathbf{H}_{SO} + \mathbf{H}_{ev}' \tag{25}$$

where $\mathbf{1}$ is the unit matrix, and the matrix $\mathbf{H}_{SO} + \mathbf{H}_{ev}$ in the basis set of the double-valued representations is presented in table 1, where E_R is the energy of the R line (see figure 1). An approximate analytical expression for E_R for the actual region of crystal-field parameters is given in [8]. For the sake of simplicity, later on we assume, as usual (see p 175 in [4]), that $\zeta_1 = \zeta_2 \equiv \lambda$.

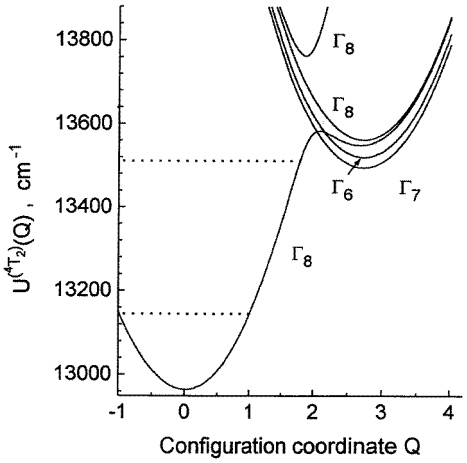

Figure 3. Adiabatic potentials of Cr^{3+} ions in $CdIn_2S_4$ single crystal, with allowance made for the spin–orbit interaction.

2.3. The dynamic vibronic problem

The spin–orbit and vibronic interactions are expressed in terms of non-commutating matrices, and therefore we arrive at the three-level pseudo-Jahn–Teller problem in the system of three quadruplet Γ_8, Γ_8', and Γ_8'' states (the $(\Gamma_8 + \Gamma_8' + \Gamma_8'') \otimes a_1$ problem). Two Kramers doublets, $\Gamma_6(^4T_2)$ and $\Gamma_7(^4T_2)$, are not mixed by the vibronic interaction either with each other or with other sublevels of $^4T_2$ and ^2E, and are shown as parallel parabolic terms, whose equilibrium position is shifted to the position Q_{T_2} with respect to the ground term $^4A_2$ (figure 1(c)). The solution of the vibronic problem for these terms is trivial:

$$\varepsilon_n(\Gamma_6) = \overline{h}\Omega_{\Gamma_6} + \overline{h}\omega\left(n + \frac{1}{2}\right) \tag{26}$$

$$\varepsilon_n(\Gamma_7) = \overline{h}\Omega_{\Gamma_7} + \overline{h}\omega\left(n + \frac{1}{2}\right) \tag{27}$$

where n is the quantum number of the harmonic oscillator, and Ω_{Γ_6} and Ω_{Γ_7} are the frequencies of the zero-phonon transitions $\Gamma_6 \to {}^4A_2$ and $\Gamma_7 \to {}^4A_2$:

$$\begin{aligned} \overline{h}\Omega_{\Gamma_6} &= 10Dq + \frac{\lambda}{4} - \frac{v^2}{2\overline{h}\omega} \\ \overline{h}\Omega_{\Gamma_7} &= 10Dq - \frac{5\lambda}{12} - \frac{v^2}{2\overline{h}\omega}. \end{aligned} \tag{28}$$

In turn, three levels, Γ_8, are mixed, and the pattern of the adiabatic curves (calculated for the set of parameters for $CdIn_2S_4$:Cr; see section 3) is rather complicated. The positions of the first two unperturbed vibrational (harmonic oscillator) levels are shown in figure 3 by the dotted lines. It can be seen that not even the first excited level can be treated in the adiabatic approximation. From this point of view, the adiabatic potential picture can be used only for visualization of the physical situation, and not to lead to any rational quantitative conclusions.

The hybrid vibronic states corresponding to the dynamic pseudo-Jahn–Teller problem $(\Gamma_8 + \Gamma_8' + \Gamma_8'') \otimes a_1$ are found as an expansion in terms of products of the zeroth-order

approximation electronic functions (the basis functions of the matrix of table 1) and functions of the non-shifted harmonic oscillator functions $\Phi_n(Q)$:

$$\Psi_v(\boldsymbol{r}, q|\Gamma_8\gamma_8) = \sum_{n=0}^{\infty}[C_{nv}(\Gamma_8)|^4\mathrm{T}_2, \Gamma_8\gamma_8\rangle + C_{nv}(\Gamma_8')|^4\mathrm{T}_2, \Gamma_8'\gamma_8\rangle + C_{nv}(\Gamma_8'')|^2\mathrm{E}, \Gamma_8''\gamma_8\rangle]\Phi_n(q). \tag{29}$$

Later, the eigenvalues and eigenvectors of the vibronic problem will be used for the evaluation of the lifetimes and luminescence band shape of $CdIn_2S_4$:Cr^{3+}.

2.4. The effective dipole moment, and the form function of the luminescence spectra

The parity-forbidden $^4\mathrm{T}_2 \rightarrow {}^4\mathrm{A}_2$ electric dipole transitions are partially allowed by the presence of a static trigonal crystal field in the host lattice $CdIn_2S_4$. The spin–orbit mixing $^4\mathrm{T}_2 \rightarrow {}^2\mathrm{E}$ makes the spin-forbidden $^2\mathrm{E} \rightarrow {}^4\mathrm{A}_2$ transition allowed, which, in this way, takes part of intensity from the $^4\mathrm{T}_2 \rightarrow {}^4\mathrm{A}_2$ transition. In the framework of the first-order perturbation theory, the effective dipole moment $\boldsymbol{D}$, taking into account the odd component of the crystal field, can be presented as

$$\boldsymbol{D} = \frac{2}{\Delta E_{eo}}\boldsymbol{P}V^{\mathrm{odd}} \tag{30}$$

where $\boldsymbol{P}$ is the dipole moment, V^{odd} is the odd-parity crystal field, and ΔE_{eo} is an effective gap between even (3d) and odd levels in the energy spectrum. In the case of D_3 symmetry, this potential is the following [3]:

$$V^{\mathrm{odd}} = \frac{2\sqrt{\pi}}{\sqrt{7}}E(r)[Y_{33}(\vartheta, \varphi) + Y_{3-3}(\vartheta, \varphi)] \tag{31}$$

where $E(r)$ is the radial part, and the spherical harmonics are quantified along the trigonal axis (figure 2(b)). The effective dipole moment can be presented in terms of circular components ($D_\pm = \mp(1/\sqrt{2})(D_X \pm \mathrm{i}D_Y)$, $D_0 = D_Z$, etc):

$$\boldsymbol{D} = -D_-\boldsymbol{k}^+ - D_+\boldsymbol{k}^- + D_0\boldsymbol{k}^0 \tag{32}$$

where

$$D_- = \frac{2}{\Delta E_{eo}}P_-V^{\mathrm{odd}} \qquad D_+ = \frac{2}{\Delta E_{eo}}P_+V^{\mathrm{odd}} \qquad D_0 = \frac{2}{\Delta E_{eo}}P_0V^{\mathrm{odd}}$$

are circular components (in the plane XY perpendicular to $C_3(Z)$, with $\boldsymbol{k}_\pm = \mp(1/\sqrt{2})(\boldsymbol{i} \pm \mathrm{i}\boldsymbol{j})$ and $\boldsymbol{k}_0 = \boldsymbol{k}$, where $\boldsymbol{i}$, $\boldsymbol{j}$, and $\boldsymbol{k}$ are the unit vectors along X, Y, and Z; see figure 2(b)). To construct the matrix for D, it is convenient to pass to the trigonal basis for d functions [4]:

$$\mathrm{t}_2 \begin{cases} x_+ = -(1/\sqrt{3})(\varepsilon\xi + \bar{\varepsilon}\eta + \zeta) \\ x_- = (1/\sqrt{3})(\bar{\varepsilon}\xi + \varepsilon\eta + \zeta) \\ x_0 = (1/\sqrt{3})(\xi + \eta + \zeta) \end{cases} \tag{33a}$$

$$\mathrm{e} \begin{cases} u_+ = -(1/\sqrt{2})(u + \mathrm{i}v) \\ u_- = -(1/\sqrt{2})(u - \mathrm{i}v) \end{cases} \tag{33b}$$

where $\varepsilon = \exp(2\pi \mathrm{i}/3)$. Now we pass to the trigonal basis in the many-electron $^4A_2(t_2^3)$ and $^4T_2(t_2^2e)$ functions. The Clebsch–Gordon coefficients for the trigonal basis of O_h are given in [3]. The results are the following:

$$\begin{aligned}
|^4A_2\rangle &= |x_0x_+x_-| \\
|^4T_2x_+\rangle &= \frac{\mathrm{i}}{\sqrt{2}}(|u_+x_-x_+| - |u_-x_0x_-|) \\
|^4T_2x_-\rangle &= \frac{\mathrm{i}}{\sqrt{2}}(-|u_-x_-x_+| - |u_+x_0x_+|) \\
|^4T_2x_0\rangle &= \frac{\mathrm{i}}{\sqrt{2}}(|u_+x_0x_-| - |u_-x_0x_+|)
\end{aligned} \tag{34}$$

where $|\cdots|$ denotes the Slater determinant ($M_S = \frac{3}{2}$). The one-electron matrix elements of D in the trigonal basis are listed in table 2, where the only semiempirical parameter, d, is expressed as follows:

$$d = \frac{\sqrt{10}}{21\,\Delta E_{eo}} e\langle rE(r)\rangle. \tag{35}$$

In equation (35), e stands for the electron charge, and $\langle\cdots\rangle$ is the mean value of $rE(r)$ calculated by means of the d functions of the $3d^3$ ion:

$$\langle rE(r)\rangle = \int_0^\infty \mathrm{d}r\ r^2 rE(r) R_{3d}^2(r).$$

Omitting the details of the calculations, we can represent the matrix elements of the effective optical transition operator $\boldsymbol{uD}$ ($\boldsymbol{u}$ is the light polarization vector) as follows:

$$\begin{aligned}
\langle\Gamma_8\gamma_S(^4A_2)|\boldsymbol{uD}|\varphi_\pm(\gamma_S)\rangle &= \frac{d}{2\sqrt{3}}(1 \mp \mathrm{i})[3\sqrt{2}\sin\vartheta\cos\varphi \pm \mathrm{i}\,3\sqrt{6}\sin\vartheta\sin\varphi - 4\cos\vartheta] \\
\langle\Gamma_8\gamma_S(^4A_2)|\boldsymbol{uD}|\zeta(\gamma_S)\rangle &= \frac{\mathrm{i}d}{\sqrt{3}}[3\sqrt{2}\sin\vartheta\cos\varphi + 2\cos\vartheta].
\end{aligned} \tag{36}$$

In equation (36), ϑ and φ are the polar coordinates of $\boldsymbol{u}$ in the coordinate system depicted in figure 2. The matrices of the operator $\boldsymbol{uD}$ for the $^4T_2(\Gamma_6\Gamma_7\Gamma_8\Gamma_8') \to {}^4A_2(\Gamma_8)$ transition can be easily obtained using equations (36) and wave-functions (4) and (5).

Table 2. One-electron matrix elements of the operator $\boldsymbol{D}$ in the trigonal basis of d-functions.

	u_+	u_-
x_+	$-\sqrt{2}dk^0$	0
x_-	0	$\sqrt{2}dk^0$
x_0	$\sqrt{2}dk^-$	0
x_+	0	$-2\sqrt{2}dk^-$
x_-	$-2\sqrt{2}dk^+$	0
x_0	0	$-\sqrt{2}dk^+$

3. Experiment and discussion

3.1. Experimental results

The model developed has been used for the description of the experimental results on the radiative characteristics of the Cr^{3+} ions in $CdIn_2S_4$:Cr single crystals. This ternary

compound is crystallized in the normal spinel structure, belonging to the O_h^7 ($Fd3m$) space group [15]. According to the EPR data, chromium ions in the trivalent state substitute for indium at the octahedral sites of the host lattice (site symmetry D_{3d} ($\bar{3}m$)) [16].

A full description of the experiment is given in [17, 18]. It should be stressed here that the results presented below were obtained for high-optical-quality $CdIn_2S_4$:Cr single crystals grown by the method of chemical transport reaction. The samples with Cr concentration in the region 0.2–0.5 at.% had the octahedral form, with natural (111)-oriented mirror-like faces, and linear sizes of 3–8 mm.

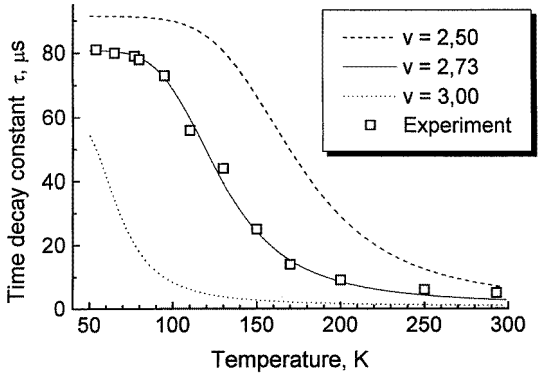

Figure 4. The temperature dependence of the decay time constant of a $3d^3$ ion in a crystal. Dashed line, solid line, and dotted line: the theoretical curves for the vibronic parameters $v = 2.50$, 2.73, and 3.00, respectively. (□: experimental measurements for $CdIn_2S_4$:Cr^{3+}.)

The experimental temperature dependence of the luminescence decay time constant for $CdIn_2S_4$:Cr crystals is shown in figure 4 by the open squares (□). The measurements have been carried out for resonant excitation of Cr^{3+} ions by pulsed radiation (pulse duration: $\tau \approx 10^{-8}$ s), the wavelength of which corresponds to the chromium impurity $^4A_2 \rightarrow {}^4T_{2g}$ absorption band, $\lambda_{ex} = 650$ nm [19].

Attention should be paid to the anomalously fast luminescence decay at low temperatures ($T \leqslant 80$ K, $\tau(R) = 8 \times 10^{-5}$ s), when the time constant is determined mainly by the lifetime of the forbidden transitions $^2E \rightarrow {}^4A_2$. As was already mentioned, the $\tau(R)$-value for trivalent chromium ions in octahedral sites is typically about $\approx 10^{-3}$ s, so $\tau(R)$ obtained for $CdIn_2S_4$:Cr is shorter by at least an order of magnitude. Figure 5(a) shows the steady-state luminescence spectra of Cr^{3+} ions in $CdIn_2S_4$:Cr, accurately measured at temperatures of 150 and 300 K (solid circles). The excitation of the steady-state luminescence, provided by a krypton-ion laser (wavelength, $\lambda_{ex} = 647$ nm), was also within the U absorption band of Cr^{3+} ions.

The experimental dependence of the emission intensity at the maximum of the U band (12×10^3 cm^{-1}), obtained by means of slow temperature scanning of the sample, is shown in figure 5(b) by open circles. In order to avoid the influence of the temperature shift of the spectral maximum, the measurements were carried out at low spectral resolution.

3.2. Discussion

The anomalous lifetime for luminescence decay seems to be an indication that the vibronic (non-adiabatic) mixing of the spin–orbit components of $^4T_2$ and ^2E plays an important role. This is exactly the case for a low barrier between the $U^{(^4T_2)}(Q)$ and $U^{(^2E)}(Q)$ potential

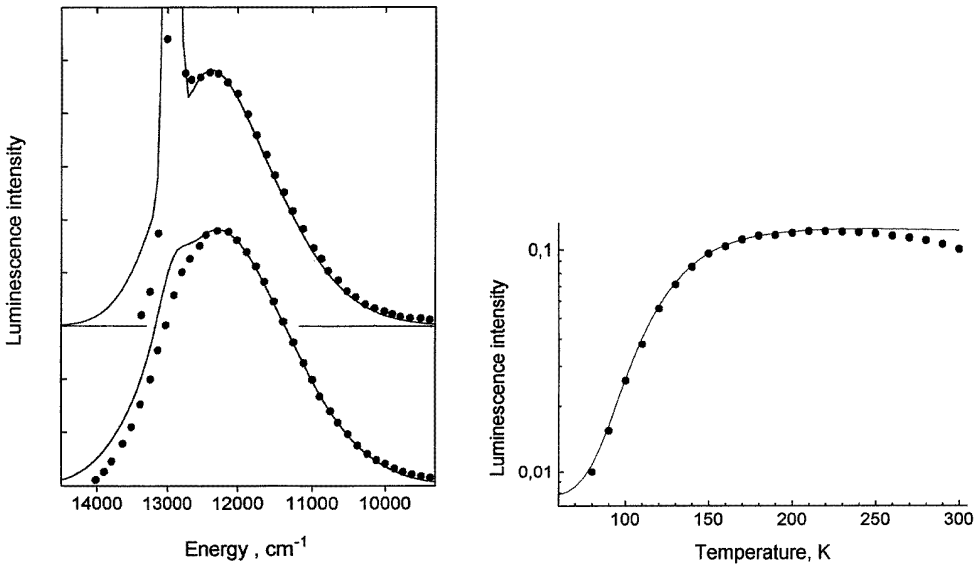

Figure 5. (a) The band shapes of the luminescence of $CdIn_2S_4$:Cr^{3+} at 150 and 300 K. (b) The U emission band intensity as a function of the temperature (solid line: theoretical calculation; circles: experimental results).

wells, when the results of the solution of the dynamic pseudo-Jahn–Teller problem are to be used. The theoretical model developed for the pseudo-Jahn–Teller effect deals with the cubic d^3 centre, taking into account an odd-parity trigonal field. Cr^{3+} ions in $CdIn_2S_4$ are affected, along with the strong cubic field of six S ions, by the weak even-parity trigonal field of six In ions in the next coordination sphere. Since the main effect of the vibronic problem is related to the pseudo-Jahn–Teller effect in a large cubic field, we will neglect the trigonal crystal field.

For numerical calculations of the vibronic Hamiltonian (equation (25), table 1), 50 unperturbed oscillator states were taken into account (general dimension of the vibronic matrix: 150×150), and the transitions were calculated between the 20 lowest states (the full number of transitions taken into account was 1200). The population of the hybrid levels in the electronically excited states is assumed to be in thermal equilibrium. According to the estimation, the chosen dimension of the basis ensures high accuracy of the evaluation of the vibronic levels populated at actual temperatures. As a result of calculations, a set of vibronic level energies of Cr^{3+} ions in $CdIn_2S_4$ have been obtained. For $CdIn_2S_4$ the following key parameters are used: $10Dq = 14\,900$ cm^{-1} [19]; $\lambda = 100$ cm^{-1}; $\overline{\hbar\omega} = 366$ cm^{-1} [20]; $E_R = 12\,960$ cm^{-1}. For this set of parameters, the vibronic levels of the $(\Gamma_8+\Gamma_8'+\Gamma_8'')\otimes a_1$ problem versus the vibronic parameter v are shown in figure 6. In the case of moderate or strong vibronic interaction, the ground state or/and the first excited states prove to be the hybrid states.

Using the eigenfunctions of the vibronic $(\Gamma_8+\Gamma_8'+\Gamma_8'')\otimes a_1$ problem (equation (29)), as well as the adiabatic solution for Γ_6 and Γ_7, one can calculate the temperature dependence of the radiative decay lifetime $\tau(T)$ as the thermal average of the reciprocal probabilities of the radiative transitions from all of the excited levels. The calculated temperature dependence of $\tau(T)$ is shown in figure 4 by the solid line. The shape of the $\tau(T)$ curve depends rather

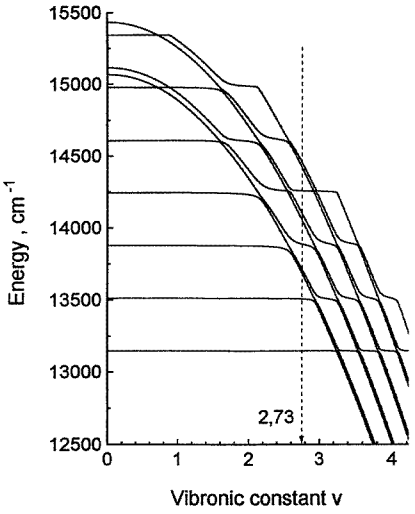

Figure 6. The vibronic spectrum of the pseudo-Jahn–Teller $(\Gamma_8+\Gamma_8'+\Gamma_8'')\otimes a_1$ vibronic problem for $CdIn_2S_4$:Cr^{3+}.

strongly on the vibronic parameter v. The influence of the spin–orbit interaction on the curve shape is much less strong, and leads mainly to the decrease of the difference between the τ-values at low and high temperatures, and to some smoothing of the curve. The best fit of the experimental data and the calculated values is achieved for $v = 2.73\overline{h}\omega$. Inspecting the vibronic levels (figure 6), one can see that at $v = 2.73\overline{h}\omega$ the ground state can be considered roughly as the harmonic oscillator level associated with the ^2E electronic state. At the same time this level has some admixture of the $^4T_2$ electronic state, and several zeroth-order vibrational states. In contrast, the first excited level (like the other levels) is a hybrid state, having a strong admixture of the excited electronic and vibrational states. One can see (figure 4) that the model of hybrid states provides full agreement of the calculated and measured decay lifetimes over a wide temperature region.

In the calculation of the form function of the luminescence band, the vibronic relaxation in the excited manifold is assumed to occur considerably more quickly than the luminescence. Considering thus the thermodynamic equilibrium population of the excited vibronic levels, one can present the form function of the luminescence band in the following form:

$$F(\Omega) = \frac{4\pi}{3\overline{h}} d^2(4+5\sin^2\theta)Z^{-1}\left(\frac{1}{\sinh(\beta/2)}[\exp(-\overline{h}\Omega_{\Gamma_6}/kT)\Pi_a(\Omega-\Omega_{\Gamma_6}) + \exp(-\overline{h}\Omega_{\Gamma_7}/kT)\Pi_a(\Omega-\Omega_{\Gamma_7})] + 2\sum_{n\nu}\exp(-\varepsilon_\nu(\Gamma_8)/kT) \times (|C_{n\nu}(\Gamma_8)|^2 + |C_{n\nu}(\Gamma_8')|^2)\delta(\varepsilon_\nu(\Gamma_8) - \overline{h}\omega\left(n+\frac{1}{2}\right) - \overline{h}\Omega)\right). \tag{37}$$

Here θ is the angle between the polarization vector of the light emitted with the frequency Ω and the trigonal axis, $\beta = \overline{h}\omega/kT$, $\varepsilon_\nu(\Gamma_8)$ are the hybrid vibronic levels of the $(\Gamma_8+\Gamma_8'+\Gamma_8'')\otimes a_1$ pseudo-Jahn–Teller problem, and Z is the statistical sum of the excited vibronic states, including both hybrid states and pure vibrational levels arising from Γ_6 and

Γ_7 (equations (27)):

$$Z = 4\sum \exp\left(-\frac{\varepsilon_\nu(\Gamma_8)}{kT}\right) + \frac{1}{\sinh(\beta/2)}\left[\exp(-\hbar\Omega_{\Gamma_6}/kT) + \exp(-\hbar\Omega_{\Gamma_7}/kT)\right]. \tag{38}$$

The first two terms in (37) represent the well known Pekar shapes of intensity distributions ('Pekarians') [11–13] corresponding to the adiabatic solutions of the electron–vibrational problem for the terms Γ_6 and Γ_7; $\Gamma_a(\Omega - \Omega_0)$ is the 'Pekarian' with the zero-phonon frequency Ω_0 and the heat-release parameter $a = v^2/\hbar^2\omega^2$ (the Pekar–Huang–Rhys parameter) [12, 13, 21]:

$$\Pi_a(\Omega - \Omega_0) = \exp\left(-\frac{a}{2}\cosh\left(\frac{\beta}{2}\right)\right) \times \sum_{n=-\infty}^{n=+\infty} \exp\left(-\frac{n\beta}{2}\right) I_n\left(\frac{a}{2\sinh(\beta/2)}\right)\delta(\hbar(\Omega - \Omega_0) - n\hbar\omega) \tag{39}$$

where $I_n(x)$ is the modified Bessel function, and the frequencies Ω_{Γ_6} and Ω_{Γ_7} of the zero-phonon lines for the $\Gamma_6 \rightarrow {}^4A_2$ and $\Gamma_7 \rightarrow {}^4A_2$ transitions, respectively, are given by equation (28).

The third term in (37) is the contribution of the transitions originating from the vibronic levels ε_ν to the full luminescence band ${}^4T_2, {}^2E \rightarrow {}^4A_2$. Since the local vibration is involved in the initial model of the impurity ion, the luminescence band shape so far obtained is described by a 'palisade' of the discrete (non-broadened) lines.

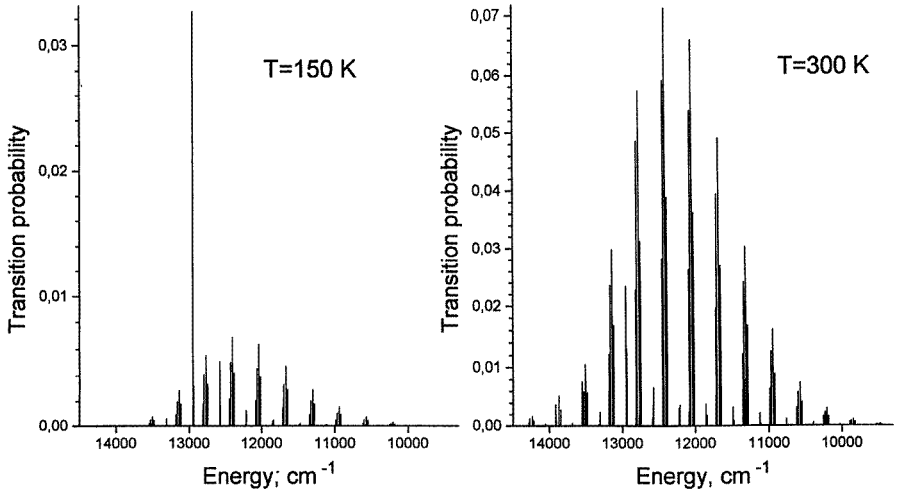

(a) (b)

Figure 7. A palisade of vibronic lines in the luminescence of $CdIn_2S_4:Cr^{3+}$ for temperatures of 150 K (a) and 300 K (b).

Figure 7 represents the luminescence spectra averaged over the directions θ at 150 and 300 K, reflecting directly the complicated irregular structure of the vibronic states. The observable optical band is smoothed due to the vibronic interaction with the continuous phonon spectrum of acoustic and optic modes. To take into account this effect, each discrete line has been replaced by a Gaussian distribution (with the half-width $\gamma = \hbar\omega$), the area of each band being equal to the intensity of the line (the probability of the corresponding

transition). A special case represents the zero-phonon R line. The intensity (area) of this line is determined by the Debye–Waller factor, and is usually weak, providing moderate or strong vibronic interaction. But, even though it is weak, this line stands out against the background of the envelope of the phonon-assisted band, due to the fact that the phonon dispersion does not contribute directly to the width of the zero-phonon line [12, 13, 21]. As one can see from the both the adiabatic potentials (figure 3) and the vibronic level pattern (figure 6), the ground vibronic level in the $^2E(\Gamma_8)$ adiabatic minimum is well isolated, and the tunnelling processes affect this level only slightly in the region of the vibronic coupling parameter $v \leqslant 2.8\overline{h}\omega$. In this region, and at relatively weak temperatures $kT < \overline{h}\omega$, the most important contribution to the R line gives the $^2E(v = 0) \rightarrow {}^4A_2(n = 0)$ optical transition, i.e. the transition between the ground vibronic levels. In the numerical simulation of the luminescence band, the half-width of this line has been taken equal to 0.2γ–0.5γ, giving rise to a sharp R peak in the full spectrum. In the calculation presented, the temperature dependence of the half-width of the R line is neglected. At the same time, the population of the excited levels in the non-equidistant vibronic spectrum gives rise to the additional significant non-uniform broadening of the zero-phonon line with the increase of temperature.

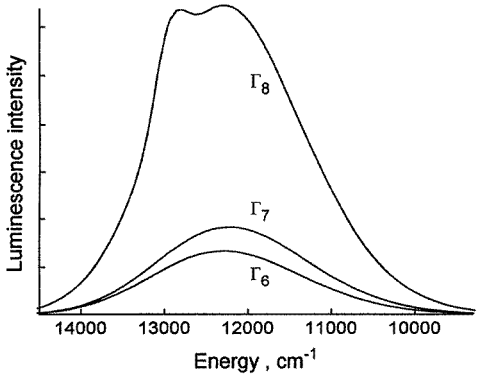

Figure 8. Contributions to the luminescence band shape from the transitions $\Gamma_8(^4T_2, {}^2E) \rightarrow {}^4A_2$, $\Gamma_6(^4T_2) \rightarrow {}^4A_2$, and $\Gamma_7(^4T_2) \rightarrow {}^4A_2$ at a temperature of 300 K.

Figure 8 shows the contributions to the luminescence bands arising from $\Gamma_8(^4T_2, {}^2E) \rightarrow {}^4A_2$, $\Gamma_6(^4T_2) \rightarrow {}^4A_2$, and $\Gamma_7(^4T_2) \rightarrow {}^4A_2$ separately. One can see that $\Gamma_8 \rightarrow {}^4A_2$ transitions contribute mainly to the full band of the luminescence. The spectral shapes of the U band, calculated for $T = 150$ K and 300 K, taking into account all three of the contributions mentioned above, are displayed in figure 5(a) by solid lines. The calculations were performed for the vibronic constant value $v = 2.73\overline{h}\omega$, providing the best fit for the decay lifetime as a function of the temperature. The calculated temperature dependence of the U emission intensity in the spectral maximum is shown in figure 5(b). A good correspondence of the theoretical curves and experimental points can be observed.

4. Conclusion

We have considered the problem of luminescence from the excited manifold ^2E, $^4T_2$ of a $3d^3$ ion in a crystal. In the case of a moderate cubic crystal field and intermediate vibronic coupling, the adiabatic approximation for the description of the excited states proves to be invalid, due to non-adiabatic mixing of three Γ_8 levels arising from $^4T_2(t_2^2e)$ and $^2E(t_2^3)$

terms. Therefore, for many crystals doped by trivalent chromium ions, the dynamic pseudo-Jahn–Teller $(\Gamma_8 + \Gamma_8' + \Gamma_8'') \otimes a_1$ problem appears. Solving this problem, we have obtained a comprehensive explanation of the temperature behaviour of the luminescence kinetic and steady-state U-emission-band intensity, as well as of the spectral shape of this band for Cr^{3+} ions in $CdIn_2S_4$ host crystals. Very good agreement of the experimental observations and theoretical calculations shows that the suggested pseudo-Jahn–Teller vibronic model of Cr^{3+} reflects the main features of physical reality. In particular, the theoretical model developed for a cubic d^3 centre gives a reasonable fit to the system possessing a trigonal component of the crystal field. It appears that the fact that the trigonal field can be of the same order of magnitude as the spin–orbit coupling is not important for the accuracy required. Moreover, incorporation of the trigonal crystal field would add two new parameters of this field ($D\sigma$ and $D\tau$ in the conventional notation; see, for example, p 117 in reference [10]). Although the local symmetry for each Cr^{3+} centre is trigonal, $D\sigma$ and $D\tau$ cannot be determined independently from polarization spectroscopy, due to presence of four trigonal equivalent positions of Cr^{3+} in the spinel lattice. This theory, possessing two additional semiempirical parameters, would be excessively flexible, and the fit to experiment could be considered artificial. For this reason, we confined ourselves to a theoretical model with the main emphasis on a large cubic field and pseudo-Jahn–Teller coupling. It should be noted at the same time that the Jahn–Teller interaction in $^4T_2(t_2^2e)$ has been neglected. Although this interaction is expected not to be strong, we intend to develop in the future a more precise model that takes into account both trigonal crystal-field and Jahn–Teller interactions in the $^4T_2$ term.

Acknowledgments

We are grateful to the referees for their helpful comments.

References

[1] Moulton P F 1985 Tunable paramagnetic-ion lasers *Laser Handbook* vol 5, ed M Bass and M L Stitch (Amsterdam: North-Holland) pp 203–288
[2] Henderson B and Imbush G F 1988 *Contemp. Phys.* **29** 235
[3] Caird J A, Payne S A, Staver P R, Ramponi A J, Chase L L and Krupke W F 1988 *IEEE J. Quantum Electron.* **24** 1077
[4] Sugano S, Tanabe Y and Kamimura H 1970 *Transition-Metal Ions in Crystals* (New York: Academic)
[5] Zhang Z, Grattan K T V and Palmer A W 1993 *Phys. Rev.* **48** 3273
[6] Yamaga M, Henderson B and O'Donnell K P 1992 *Phys. Rev.* **46** 3273
[7] Yamaga M, Henderson B and O'Donnell K P 1989 *J. Phys.: Condens. Matter* **1** 9175
[8] Yamaga M, Henderson B, O'Donnell K P, Cowan C T and Marshall A 1990 *J. Appl. Phys.* B **50** 425
[9] Yamaga M, Henderson B, O'Donnell K P and Yue G 1990 *J. Appl. Phys.* B **51** 132
[10] Tsukerblat B S 1994 *Group Theory in Chemistry and Spectroscopy. A Simple Guide to Advanced Usage* (London: Academic)
[11] Koster G F, Dimmock J O, Wheeler R G and Statz H 1963 *Properties of the Thirty-Two Point Groups* (Cambridge, MA: MIT Press)
[12] Perlin Yu E and Tsukerblat B S 1984 Optical bands and polarization dichroism of Jahn–Teller centers *Dynamical Jahn–Teller Effect in Localized Systems* ed Yu E Perlin and M Wagner (Amsterdam: Elsevier) pp 251–346
[13] Perlin Yu E and Tsukerblat B S 1974 *Electron–Vibrational Interactions in the Optical Spectra of Impurity Paramagnetic Ions* (Kishinev: Stiinta) (in Russian)
[14] Muramatsu S and Sakamoto N 1979 *J. Phys. Soc. Japan* **46** 1273
[15] Czaja W 1970 *Phys. Condens. Mater.* **10** 299
[16] Henning J C M, Bongers P F, Van Den Boom and Voermans A B 1969 *Phys. Lett.* **30A** 307

[17] Kulikova O V, Kulyuk L L, Popov S M, Strumban E E, Tezlevan V E, Bove J and Fortin E 1992 *Fiz. Tverd. Tela* **34** 1907
[18] Kulikova O V, Kulyuk L L, Popov S M and Tezlevan V E 1993 *Japan. J. Appl. Phys. Suppl.* 3 **32** 484
[19] Ueno M 1979 *J. Phys. Soc. Japan* **46** 1887
[20] Gubanov V A, Kulikova O V, Kulyuk L L, Radautsan S I, Ratseev S I, Salivon G I, Tezlevan V E and Tsisanu V I 1988 *Fiz. Tverd. Tela* **30** 457
[21] Perlin Yu E 1963 *Sov. Phys.–Usp.* **6** 983